

Image reconstruction by backprojection from frequency-domain optical measurements in highly scattering media

Scott A. Walker, Sergio Fantini, and Enrico Gratton

The reconstruction of the location and optical properties of objects in turbid media requires the solution of the inverse problem. Iterative solutions to this problem can require large amounts of computing time and may not converge to a unique solution. Instead, we propose a fast, simple method for approximately solving this problem in which calculated effective absorption and reduced scattering coefficients are backprojected to create an image of the objects. We reconstructed images of objects with centimeter dimensions embedded in a diffusive medium with optical characteristics similar to those of human tissue. Data were collected by a frequency-domain spectrometer operating at 120 MHz with a laser diode light source emitting at 793 nm. Intensity and phase of the incident photon density wave were collected from linear scans at different projection angles. Although the positions of the objects are correctly identified by the reconstructed images, the optical parameters of the objects are recovered only qualitatively. © 1997 Optical Society of America

Key words: Backprojection, image reconstruction, photon migration, frequency domain, tomography, near infrared.

1. Introduction

In the red and near-infrared (NIR) wavelength regions of the optical spectrum (650 to 1300 nm), absorption of light by human tissues is low enough that a measurable flux of diffusely transmitted or reflected light can be collected from volumes centimeters below the skin surface. Diffuse light transmission allows for the possibility of obtaining spatial reconstructions of the optical properties of effluent regions within the tissue, known as NIR imaging. Techniques that employ NIR imaging are noninvasive, safe, cost-effective diagnostic tools in clinical studies. Because NIR photons travel diffusively between source and detector, they probe a relatively large region between the source and the detector rather than a straight line, as in the x-ray case.

Recent advances in laser technology and in the theoretical understanding of light propagation in tissues have encouraged efforts to explore methods for

image reconstruction. As a result, considerable progress has been made, including the development of time-resolved techniques that have been successfully employed in both the frequency and the time domains to separate and accurately measure the optical absorption and reduced scattering coefficients (μ_a and μ_s' , respectively) in macroscopically homogeneous turbid media.^{1,2} Also it has been shown that optical inhomogeneities can be detected from 1 to 5 cm below the tissue surface by the use of time-resolved techniques in a reflection geometry.³

Many researchers have proposed to apply time-resolved measurement techniques and a better theoretical understanding of photon propagation in homogeneous media to heterogeneous systems. New models have been developed for iteratively solving the inverse problem both experimentally⁴ and through numerical modeling.⁵⁻¹¹ Most of the numerical inversion techniques are based on the diffusion approximation of the Boltzmann transport equation, although some new methods attempt to apply the transport equation directly. These algorithms can in principle detect, locate, and characterize optical inhomogeneities quantitatively. Although these are valuable long-range goals for NIR imaging, these computer-reconstruction methods currently have weak points in that there is no guarantee that the algorithm will converge to a unique solution, and so-

The authors are with the Department of Physics, Laboratory for Fluorescence Dynamics, University of Illinois at Urbana-Champaign, 1110 West Green Street, Urbana, Illinois 61801-3080.

Received 8 February 1996; revised manuscript received 5 July 1996.

0003-6935/97/010170-10\$10.00/0

© 1997 Optical Society of America

lutions can be sensitive to uncertainties in the experimental measurements.

For the purpose of image reconstruction, we propose a hybrid approach in which we first determine the reduced scattering and absorption coefficients of the medium in a relatively small volume around the source–detector line. We calculate the average reduced scattering and absorption coefficients for a volume defined by the photon trajectories that connect source and detector in the medium. The calculation employs equations derived from the diffusion approximation to the Boltzmann transport equation for a macroscopically homogeneous medium. Our approach is then to backproject scattering and absorption parameters of the medium, which are measured in the frequency domain. In the frequency domain, data gathered at a single point consist of the phase, average intensity (dc), and amplitude (ac) of the photon density wave generated by an intensity-modulated source. We have demonstrated that after calibration of the light source on a medium of known optical properties, it is possible to calculate the optical properties of an unknown homogeneous medium from a single point measurement.¹² For the phantom media, we treat inhomogeneities as a perturbation to the homogeneous case and calculate local values of the absorption and reduced scattering coefficients from a measurement of the perturbed photon density wave. The reconstruction algorithm is similar to backprojection algorithms used for conventional computed tomography (CT). This method has the advantages in that it always gives a unique image and requires less computational time than iterative techniques. We discuss the motivation for calculating physical parameters (i.e., absorption and scattering) rather than employing only measured dc and phase values and evaluate the spatial resolution of this technique relative to the dc case.

2. Theoretical Background

A. Calculation of Optical Coefficients

The model used to describe light propagation in scattering media, such as human tissue, makes use of the Boltzmann transport equation. Starting from the diffusion approximation to the Boltzmann transport equation, it is possible to derive the frequency-domain quantities U_{dc} (the average photon density), U_{ac} (the amplitude of the photon density oscillations), and Φ (the phase of the photon density oscillations) for a sinusoidally intensity-modulated light source in a macroscopically homogeneous, strongly scattering, infinite medium¹³:

$$U_{dc} = \frac{S}{4\pi\nu D} \frac{\exp\left[-r\left(\frac{\mu_a}{D}\right)^{1/2}\right]}{r}, \quad (1)$$

$$U_{ac} = \frac{SA}{4\pi\nu D} \frac{\exp[r \operatorname{Re}(k)]}{r}, \quad (2)$$

$$\Phi = r \operatorname{Im}(k) + \Phi_s, \quad (3)$$

where

$$k = -\left(\frac{\mu_a}{D} - \frac{i\omega}{\nu D}\right)^{1/2}, \quad (4)$$

$$D = 1/3\mu'_s \text{ (Ref. 14)}. \quad (5)$$

Here ν is the speed of light in the medium, μ_a and μ'_s are the absorption and the reduced scattering coefficients of the medium, respectively, ω is the angular-modulation frequency of the source, S is the source strength (in units photons/per second), A is the source modulation (ratio of ac to dc components of the source intensity), and Φ_s is the phase source term. Unknowns in these expressions include the source terms S , A , and Φ_s along with the optical coefficients μ_a and μ'_s . It has been shown that values of μ_a and μ'_s can be determined in a homogeneous medium by the use of a reference measurement on a medium of known optical properties.¹²

Because we are interested in determining the optical properties for a heterogeneous medium, Eqs. (1)–(5) are not strictly applicable. Hence the values calculated for μ_a and μ'_s from Eqs. (1)–(5) can only be termed effective absorption and reduced scattering coefficients. However, we can proceed on the hypothesis that these parameters still contain useful information about heterogeneities in a highly scattering background medium if the perturbation to the homogeneous case is small. Although small inhomogeneities with optical properties similar to those of the background can be treated as perturbations to the homogeneous medium equations,^{15,16} even larger inhomogeneities that do not fall within the range of the perturbation theory can be reconstructed in qualitatively correct images.

B. Filtered Backprojection

Data are taken at a constant source–detector separation with both source and detector scanning across the entire reconstruction region. After we obtain effective values of μ_a and μ'_s from Eqs. (1)–(5), we apply backprojection techniques commonly used for x-ray CT to obtain reconstructed images. As opposed to iterative techniques, the values of effective absorption and reduced scattering coefficients from each measurement are projected back, in a single step, along the region between source and detector by the use of an appropriate weight function. An image is formed by the averaging of data from source–detector scans taken at multiple angles. Because photons travel diffusively from source to detector, the choice of an appropriate weight function is not obvious. We choose a straight line, as in x-ray CT, to locate objects correctly in the turbid medium with minimum computational effort.

The finite number of measurements in a reconstruction leads to a filtered backprojection technique. Here the filtering weight function¹⁷ for a projection

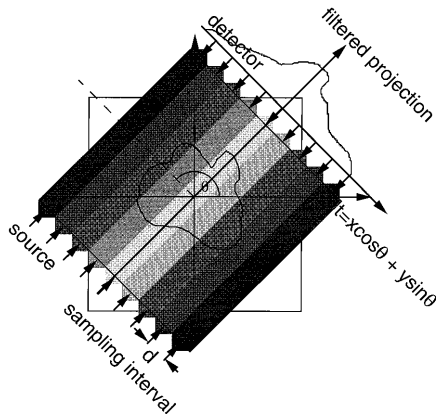


Fig. 1. X-ray weight function is filtered to account for the size of the sampling period d . Filtered values are then projected back along the source–detector ray for a projection at angle θ . After this step the projections at all angles θ are summed.

taken at angle θ is defined as

$$h(t) = \frac{1}{2d} \frac{\sin p}{p} - \frac{1}{4d} \left(\frac{\sin \frac{p}{2}}{\frac{p}{2}} \right)^2, \quad (6)$$

where $p = (\pi t)/d$ and $t = x \cos \theta + y \sin \theta$. The shape of the weight function $h(t)$ depends on only the sampling interval d used to acquire the data in each projection. We note that the FWHM of $h(t)$ in our case is roughly 10 times smaller than the width of the volume sampled by photons traveling from source to detector. This weight function is convoluted with the measured values in each projection to derive continuous images from discrete measurements in the image plane (see Fig. 1):

$$\mu_{\theta}^f(t) = \int_{-\infty}^{\infty} \mu_{\theta}^m(t') h(t - t') dt'. \quad (7)$$

Here $\mu_{\theta}^m(t)$ stands for the measured data for a projection at angle θ , and $\mu_{\theta}^f(t)$ is that projection filtered by the function $h(t)$. Finally, the contributions from projections at each angle are added together to give the reconstructed image with spatial coordinates (x, y) :

$$\mu^*(x, y) = \int_0^{\pi} \mu_{\theta}^f(x \cos \theta + y \sin \theta) d\theta. \quad (8)$$

The backprojection techniques used here should be differentiated from the methods used by Barbour *et al.*¹⁸ Barbour *et al.*'s method employs perturbation theory (based on the assumption of small perturbations to an initial homogeneous map of optical coefficients) to solve the forward problem, thereby creating a model system that is iteratively modified in order to minimize the differences between simulated data and experimental data. Our backprojection scheme makes no attempt to generate a model

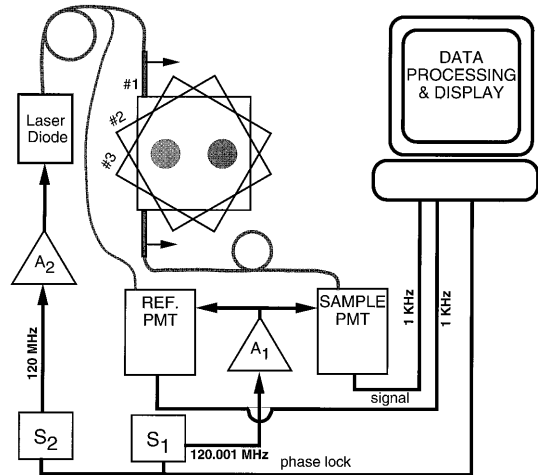


Fig. 2. Block diagram of the frequency-domain instrumentation. A 120-MHz radio frequency signal generated by synthesizer S_2 is amplified by amplifier A_2 and sent to the 793-nm laser diode, producing 50 mW of output light that is then coupled with a 20% efficiency into a fiber-optic conduit, giving an output power in the medium of 10 mW. A small fraction of the light is sent to a reference photomultiplier tube (PMT) to correct for source intensity fluctuations. The output light produces a photon density wave that is perturbed by the objects. The multiply scattered light is collected by a fiber-optic bundle that is connected to a sample PMT. A cross-correlation electronics system processes the PMT signal by using a 1-KHz signal generated by synthesizer S_1 and amplified by A_1 . The measurement is repeated 41 times as the source and detector are scanned across the area of interest in the direction of the arrows. After scan #1 the scanning direction is rotated 30° relative to its original position and the scan is repeated. The data for each slice consist of seven projections at 30° increments from 0° to 180°.

system by solving the forward problem. Instead, with the purpose of developing a fast imaging tool, we employ the Radon transform to directly obtain a qualitative, calibrated (see Fig. 4) reconstruction of the region of interest.

3. Methods

The experimental measurements were conducted in a quasi-infinite geometry with a frequency-domain spectrometer¹⁹ and an XYZ positioning scanner (see Fig. 2). Briefly, a 120-MHz radio frequency signal is amplified and sent to a 50-mW laser diode coupled to a 1-mm fiber-optic conduit to channel the NIR light into the turbid medium. The coupling efficiency with the laser diode is 20%, giving an output power of 10 mW. A small fraction of the output light is sent to a reference photomultiplier tube (R928 Hamamatsu) to correct for drift or intensity fluctuations in the source. Detected light is collected by a 0.3-cm-diameter fiber-optic bundle and processed with frequency-domain methods¹⁹ (cross-correlation frequency 1 kHz) to measure the dc intensity, ac amplitude, and phase of the photon density wave. This process is repeated as the source and detector are scanned across the measurement area. Each scan takes place inside a large glass container of Intralipid fat emulsion (Liposin III from Abbott Laboratories,

Table 1. Size and Optical Properties of Background Medium and Objects

Object Type	Size	Number of Objects	μ_a (cm ⁻¹)	μ'_s (cm ⁻¹)
Background medium (Intralipid + India ink)	16-L total volume		0.079 ± 0.005	7.9 ± 0.1
Cylindrical object A- (hot melt glue)	1.5-cm diameter	1	0.045 ± 0.003	7.5 ± 0.5
	1.0-cm diameter	2		
Cylindrical object A+ (hot melt glue)	1.5-cm diameter	1	0.13 ± 0.01	8.0 ± 0.5
	1.0-cm diameter	2		

Chicago, Ill.) mixed with black India ink. The volume of the container is 16 L. The concentrations of Intralipid and India ink are adjusted to give optical coefficients $\mu_{a0} = 0.079 \text{ cm}^{-1}$, $\mu'_{s0} = 7.9 \text{ cm}^{-1}$ ($\lambda_{\text{source}} = 793 \text{ nm}$) as measured by a multidistance protocol.² These values of μ_{a0} and μ'_{s0} match typical values of soft tissue in the NIR.

To introduce inhomogeneities with optical properties different from those of the background medium, we cast six cylindrical objects (10 cm long, four with a diameter of 1.0 cm, two with a diameter of 1.5 cm) from hot-melt glue (Arrow Fastener Co., Saddle Brook, N.J.) mixed with varying amounts of India ink. The optical properties of each object were measured from a large block of the same material by the use of a semi-infinite measurement protocol.²⁰ Optical properties of the objects and of the background medium are shown in Table 1.

The reduced scattering coefficients of all six objects match those of the background medium. Three objects are less absorbing than the background (and are identified as A-), whereas three are more absorbing (and are identified as A+). Single cylinders of types A- and A+ with a diameter of 1.5 cm were scanned in a single projection to obtain Figs. 3(a) and 3(b). 1.0-cm-diameter cylinders were scanned as single cylinders (Figs. 4 and 5), two cylinders of the same ma-

terial (Figs. 6 and 7), and two cylinders of different materials (Fig. 8).

The cylinders were positioned vertically with respect to the scanning plane in the Intralipid mixture at different angles relative to the source-detector scan direction (see Fig. 9) by means of a glass rod (0.3-cm diameter) connected to a rotational stage. The cylinders, which were twice the length of the source-detector separation, were effectively treated as infinite cylinders, and we verified that the glass rod does not affect the measurements.

The reconstructions employed data taken in seven projections at 30° angle increments from 0° to 180° around the region of interest. Each projection employed a linear scan with source and detector facing each other at a separation of 5 cm. The scan consisted of 41 measurement points at 0.2-cm steps for a total scan length of 8 cm. Because the source-detector separation was 5 cm, only the central 5 cm of the scan length were actually used in reconstructing the images. Values of the effective absorption and reduced scattering coefficients were calculated for each point, by the use of Eqs. (1)–(5), and a reference measurement in the absence of inhomogeneities. An image of the object was then reconstructed by filtered backprojection of the effective μ_a and μ'_s op-

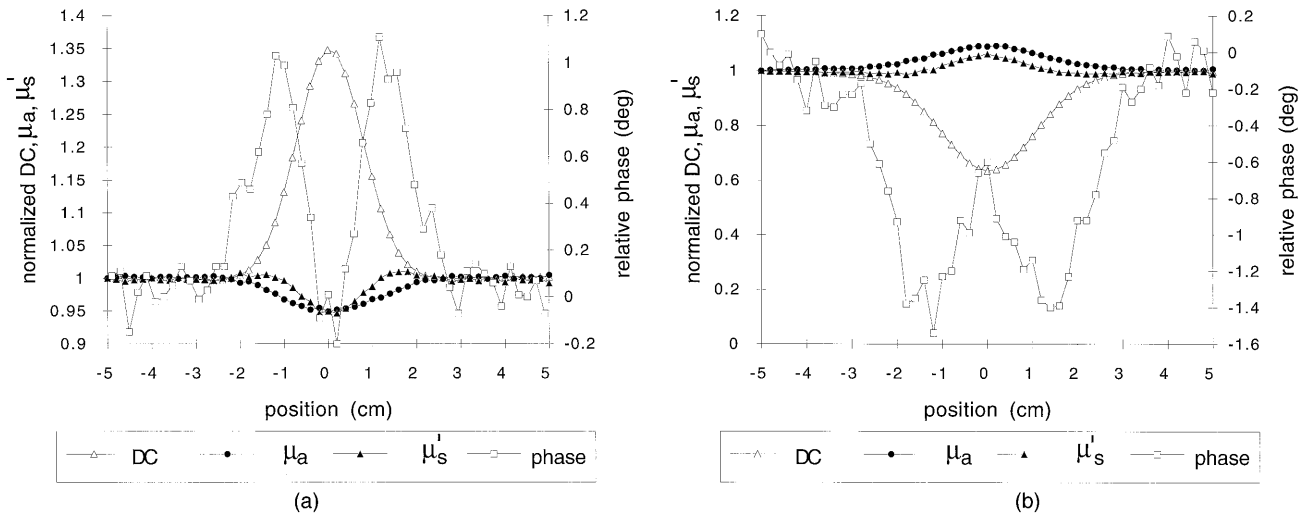


Fig. 3. Comparison of directly measured parameters, phase, and dc, with calculated values of effective μ_a and μ'_s for 1.5-cm-diameter cylinders immersed in a highly scattering background medium ($\mu'_{s0} = 7.9 \pm 0.1 \text{ cm}^{-1}$, $\mu_{a0} = 0.079 \pm 0.005 \text{ cm}^{-1}$). (a) Type A- cylinder is less absorbing than the background, (b) type A+ cylinder is more absorbing than the background. The parameters dc, effective μ_a , and effective μ'_s are shown in normalized units to illustrate the differences in contrast and sharpness of the perturbation caused by the cylinder. The two peaks in the phase plots are due to the distortion of the photon density wave front by each cylinder.

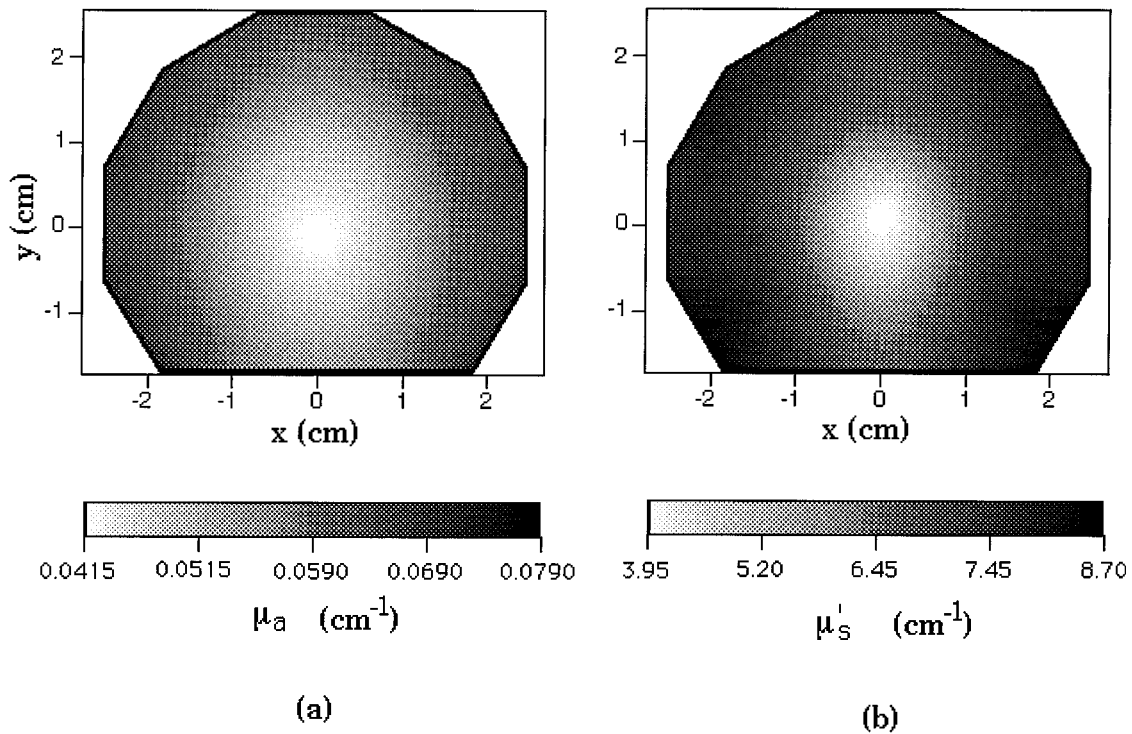


Fig. 4. Reconstructed images of calculated parameters, effective μ_a and μ'_s , for a 1.0-cm-diameter, type A- cylinder ($\mu_a = 0.045 \pm 0.03 \text{ cm}^{-1}$) immersed in a highly scattering background medium ($\mu'_s = 7.9 \pm 0.1 \text{ cm}^{-1}$, $\mu_a = 0.079 \pm 0.005 \text{ cm}^{-1}$). (a) Effective μ_a image, (b) effective μ'_s image. Each image is reconstructed from seven projections taken at 30° intervals from 0° to 180° . The reconstruction region is shown by the thick black line. All images are scaled by calibration factor $c = 25 [\mu_{\text{image}} = (\mu^* - \mu_{\text{background}}) c + \mu_{\text{background}}]$.

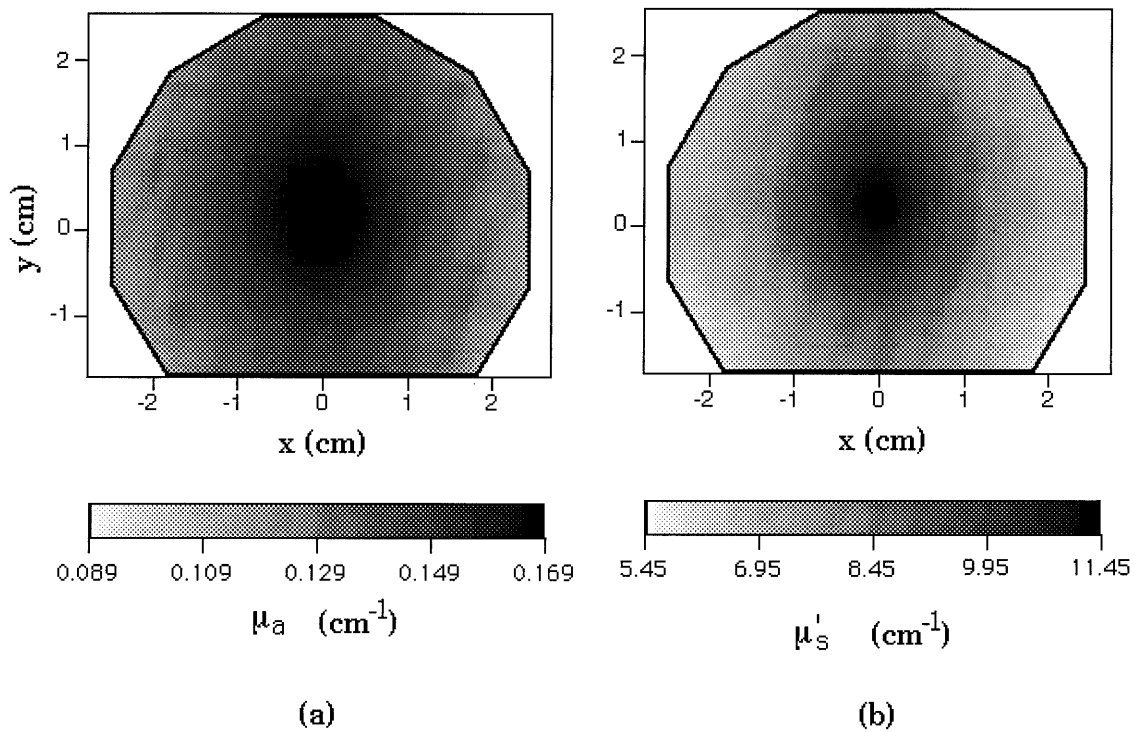


Fig. 5. Reconstructed images of calculated parameters, effective μ_a and μ'_s , for a 1.0-cm-diameter, type A+ cylinder ($\mu_a = 0.13 \pm 0.01 \text{ cm}^{-1}$) immersed in a highly scattering background medium ($\mu'_s = 7.9 \pm 0.1 \text{ cm}^{-1}$, $\mu_a = 0.079 \pm 0.005 \text{ cm}^{-1}$). (a) Effective μ_a image, (b) effective μ'_s image. Each image is reconstructed from seven projections taken at 30° intervals from 0° to 180° . The reconstruction region is shown by the thick black line.

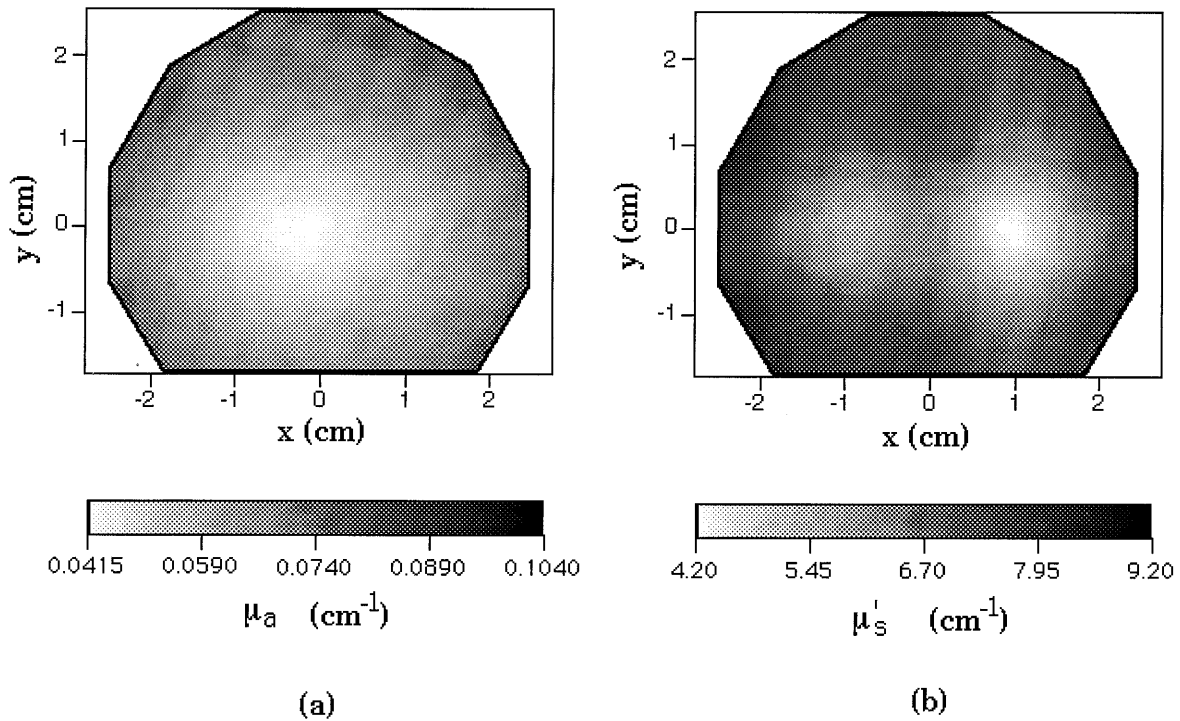


Fig. 6. Reconstructed images of calculated values, effective μ_a and μ'_s , for two 1.0-cm-diameter, type A- cylinders ($\mu_a = 0.045 \pm 0.03 \text{ cm}^{-1}$), centers located at (-1 cm, 0 cm) and (1 cm, 0 cm). Both cylinders were immersed in a highly scattering background medium ($\mu'_s = 7.9 \pm 0.1 \text{ cm}^{-1}$, $\mu_a = 0.079 \pm 0.005 \text{ cm}^{-1}$). (a) Effective μ_a image, (b) effective μ'_s image. In the effective μ'_s images the two cylinders are resolved whereas in the effective μ_a images they are not.

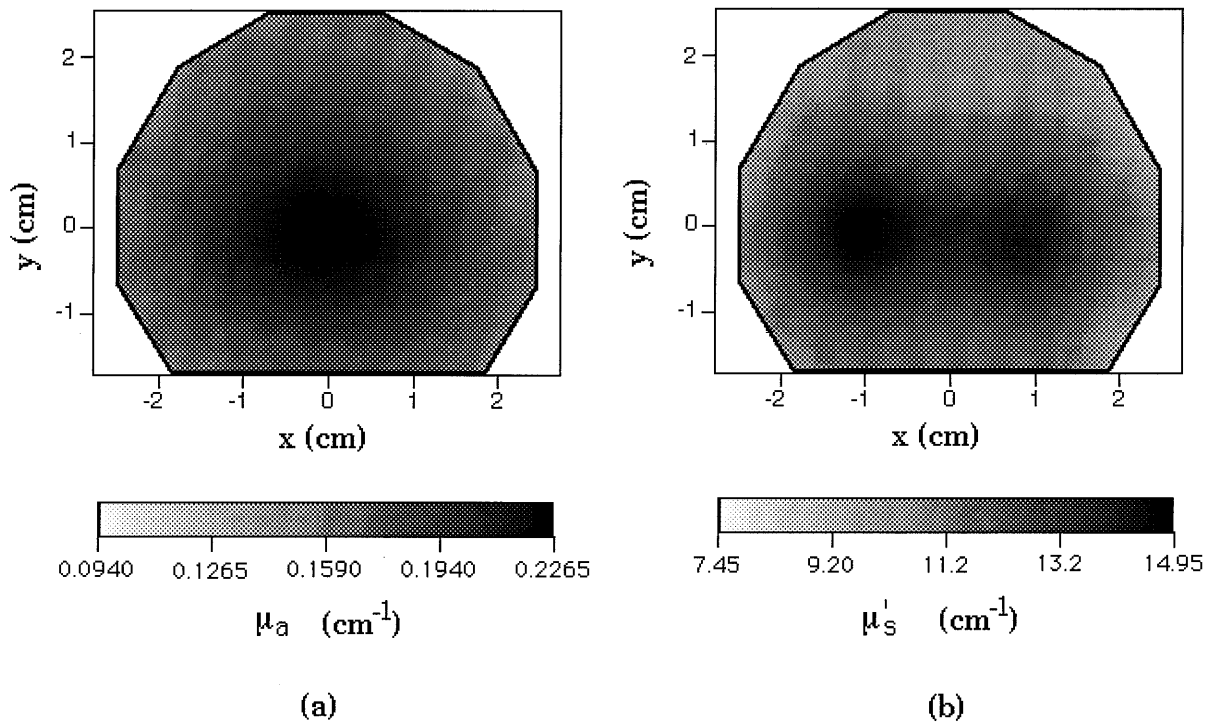


Fig. 7. Reconstructed images of calculated values, effective μ_a and μ'_s , for two 1.0-cm-diameter, type A+ cylinders ($\mu_a = 0.13 \pm 0.01 \text{ cm}^{-1}$), centers located at (-1 cm, 0 cm) and (1 cm, 0 cm). Both cylinders were immersed in a highly scattering background medium ($\mu'_s = 7.9 \pm 0.1 \text{ cm}^{-1}$, $\mu_a = 0.079 \pm 0.005 \text{ cm}^{-1}$). (a) Effective μ_a image, (b) effective μ'_s image. In the effective μ'_s images the two cylinders are resolved whereas in the effective μ_a images they are not.

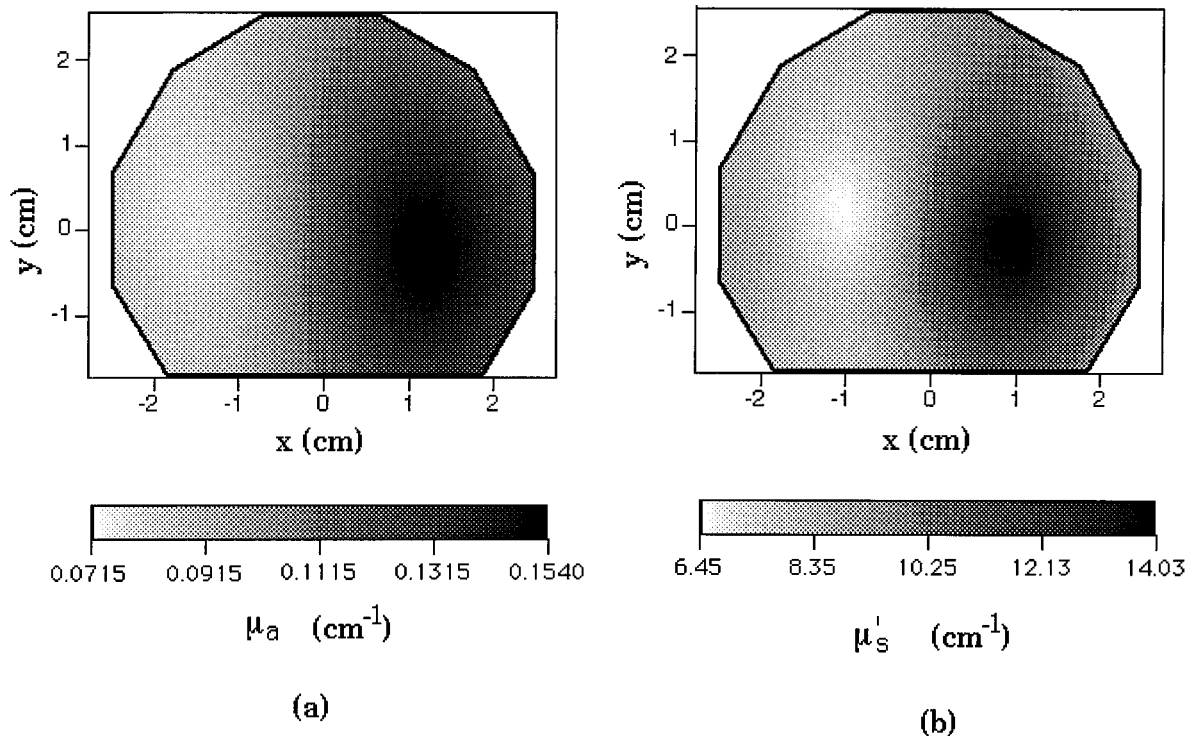


Fig. 8. Reconstructed images of calculated values, effective μ_a and μ'_s , for two 1.0-cm-diameter cylinders, centers located at $(-1 \text{ cm}, 0 \text{ cm})$ and $(1 \text{ cm}, 0 \text{ cm})$. (a) The left cylinder is less absorbing than the background medium (type A-) whereas the right cylinder is more absorbing than the background medium (type A+). The values of the objects are recovered qualitatively correctly in the effective μ_a map. (b) The increased resolution of the effective μ'_s images allows a more accurate determination of the cylinder positions.

tical coefficients, separately, as described in Subsection 2.B.

4. Results

The time required for reconstructing a complete two-dimensional image of effective μ_a and μ'_s from a set of seven projections of 41 measurements each is roughly

5 s on a 66-MHz 486 personal computer. This time includes the calculation of effective μ_a and μ'_s from the phase and intensity measurements, application of the filtering function, and integration over all projections. As in x-ray backprojection, the image can be constructed in parallel with data acquisition, thus decreasing the total time to generate an image.

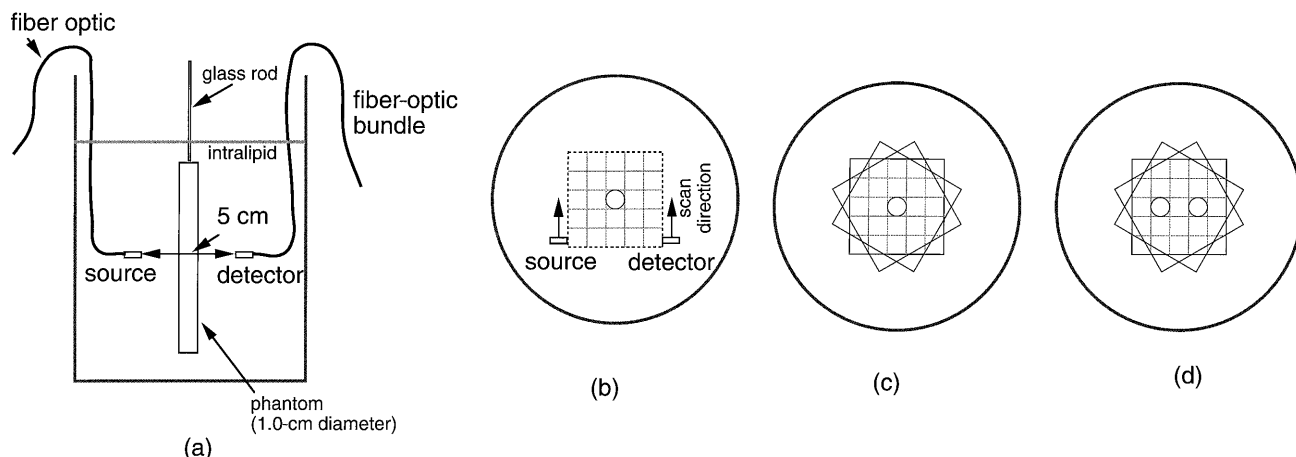


Fig. 9. Experimental setup. (a) Side view of the 16-L glass container filled with Intralipid/India ink mixture. Fiber optics carry light from the source and to the detector. The fiber tips are separated by 5 cm inside the tank and scanned by means of an XYZ positioning scanner. The object is suspended in the scattering medium by a 3-mm-diameter glass rod. (b) Top view of cylindrical object. The source and the detector make a one-dimensional scan perpendicular to the object across the volume of interest. (c) Top view of multiple projections measured on a single object. Each square denotes a separate projection. In our measurements, projection angles ranged from 0° to 180° in 30° steps. (d) Top view of multiple projections measured on two cylindrical objects.

Table 2. Contrast and FWHM of Single-Cylinder Calibrated Images with a Diameter of 1.0 cm

Type	C_{dc} (%)	C_{μ_a} (%)	$C_{\mu'_s}$ (%)	FWHM _{dc} (cm)	FWHM _{μ_a} (cm)	FWHM _{μ'_s} (cm)
A+	438	100	68	3.0	3.8	1.9
A-	275	38	50	3.0	3.0	1.4

To compare the reconstructed images below, we define contrast C_x for a specific quantity x as:

$$C_x = \frac{|x_{\text{peak}} - x_{\text{background}}|}{x_{\text{background}}}. \quad (9)$$

Given two objects with the same size and optical properties, we can say that they are resolved when their reconstructed image shows two maxima separated by a minimum located between the objects. We can define the resolution of the imaging technique as the distance between the centers of two objects barely resolved (i.e., the difference between minimum and maxima is greater than the measurement noise). If the two objects give independent contributions to the reconstructed image, the distance at which they are resolved is equal to the FWHM of the image of either object measured separately. Thus the FWHM for a single object can be regarded as a rough estimate of the resolution of this technique. Also, we introduce a quantity called relative resolution, which is defined as

$$R_x = \frac{(x_{\text{peak1}} + x_{\text{peak2}})/2 - x_{\text{min}}}{x_{\text{mm}} C_x}, \quad (10)$$

where x_{min} represents the minimum value midway between the two peaks. This definition compares the depth of the minimum that separates two similar objects with the contrast of the image. If these two quantities are equal, the relative resolution is 100%.

We concentrate on the case of inhomogeneities with absorption different from that of the background. First we describe the raw data and the calculated parameters for a single projection, and then we compare contrast and FWHM for images of effective μ_a and μ'_s with single objects of types A- and A+. We evaluate the resolution for a medium containing two objects of the same type (either A- or A+) by using both a reconstructed image and a cross section of that image. Finally, this reconstruction method is evaluated for two objects of different absorption parameters (types A- and A+ together).

A. Single Projection

Figure 3(a) shows the raw data and effective absorption and reduced scattering coefficients for a cylindrical object of type A- with a diameter of 1.5 cm. The values of the phase and dc of the measured intensity are similar to the background values far away from the object. The dc trace shows a peak, located at the center of the object, that is considerably broader than the object itself (1.9 cm FWHM). The phase shows a double peak with a phase difference of $\sim 1^\circ$. This

structure is due to the diffraction and refraction of the photon density wave and has been measured both for partially^{4,21,22} and totally²³ absorbing objects. Note that the phase decreases below the background value but this does not affect the sign of either effective μ_a or μ'_s . In fact, the calculated values of μ_a and μ'_s both have shapes similar to the dc intensity with minima at the position of the object. Although μ_a and μ'_s have smaller contrasts than the dc intensity (type A-: $C_{dc} = 35\%$, $C_{\mu_a} = 5\%$, $C_{\mu'_s} = 5\%$), the μ_a projection has a larger FWHM (2.4 cm) and the μ'_s projection has a smaller FWHM (1.5 cm) than the dc intensity. Figure 3(b) shows the same information for an object of type A+ with a diameter 1.5 cm. The dc trace exhibits the same contrast as in the type A- case; however, the phase increases to $\sim 1.4^\circ$, thus increasing the contrast of the effective μ_a and μ'_s traces (type A+: $C_{dc} = 37\%$, $C_{\mu_a} = 9.0\%$, $C_{\mu'_s} = 7.0\%$).

Note that the effective μ_a and μ'_s traces have similar contrasts, even though the measured objects have reduced scattering coefficients that are within 6% of the background values whereas the absorption coefficients of the objects are 57% or 165% of the background. We expect the values of effective μ_a and μ'_s to be interdependent to some extent as they are based on homogeneous infinite-medium equations. The size of the perturbation caused by each object depends on the object's dimensions and difference in optical properties from those of the background medium. Finally, because of the experimental difficulties of producing each object, the values of the scattering coefficients of the objects can be as much as 12% different from the background values. This difference could contribute to part of the correlation between effective μ_a and μ'_s traces.

B. Single-Cylinder Reconstruction

The reconstructed images in Fig. 4 represent reconstructions of a single cylindrical object of type A- with a diameter of 1.0 cm. The gray scales are bounded by the minimum and the maximum values of the reconstructed images. Lighter regions denote areas of lower effective absorption and lower effective reduced scattering coefficients. The valid reconstruction region (where all the projections overlap) is shown by the thick black line. Figure 5 represents the same images generated for an object of type A+ with a diameter of 1.0 cm. Although the μ'_s images have a similar contrast to that of the μ_a images (see Table 2), in both the type A- and type A+ cases the image of effective μ'_s is sharper than the effective μ_a image (see Table 2). The fact that the map of effec-

Table 3. Contrast and Relative Resolution of Two-Cylinder Images with a Diameter of 1.0 cm

Type	C_{dc} (%)	C_{μ_a} (%)	$C_{\mu'_s}$ (%)	R_{dc} (%)	R_{μ_a}	$R_{\mu'_s}$ (%)
A+, A+	650	190	78	—	—	12
A-, A-	350	75	50	7.1	—	41

tive μ_a and effective μ'_s could significantly differ in terms of resolution has been previously suggested.²⁴

C. Two Cylinders: Same Absorption

Figures 6 and 7 show reconstructions of two 1.0-cm-diameter cylinders of the same absorption and reduced scattering coefficients with centers separated by 2.0 cm. The effective μ_a reconstruction of the less-absorbing objects A- in Fig. 6 show a single dip between centers of the objects whereas the cylinders in the effective μ'_s images are clearly distinguishable. The fact that the minima corresponding to the objects in the effective μ'_s reconstruction are not equal could be due to slight differences in the objects' absorption and scattering properties. Similarly, Fig. 7 shows that the type A+ objects are unresolved in the effective μ_a image and resolved in the effective μ'_s image. The contrast and resolution in these images are reported in Table 3.

D. Two Cylinders: Different Absorption

Figure 8 shows the performance of measured and calculated parameters for two cylinders of similar reduced scattering coefficients, but with one cylinder less absorbing and the other cylinder more absorbing than the background medium. The type A- cylinder is easily visible in the effective μ'_s reconstruction.

5. Discussion

In this paper we have presented an image-reconstruction scheme based on backprojection of the calculated effective absorption and reduced scattering parameters of the medium measured at a single source-detector position. This scheme represents an experimental approach adapted from x-ray tomography. Images were reconstructed of objects with centimeter dimensions that have optical characteristics similar to those of human tissue. Both single and multiple inhomogeneities were measured with similar optical scattering parameters and with absorption parameters greater and less than background values.

Backprojection has the advantage in that it can produce images quickly, employing relatively few computational resources compared with iterative techniques. This makes it ideal for use in real time, in conjunction with a noninvasive monitor. Because of the approximations that are made to adapt the linear theory of x-ray backprojection to the nonlinear propagation of diffusing photons, the method described in this paper is not strictly applicable. However, for the cases considered, the reconstructed images of μ_a are qualitatively correct. In the presence of both single and multiple objects of different

absorptions, both the position and the qualitative nature (more absorbing, less absorbing) of the inhomogeneity are correctly reconstructed. Also, it is possible to use extra information derived from time-resolved measurements to generate parameters (such as effective μ'_s) that have a higher resolution than reconstructions of the intensity (represented by the dc measurements in this paper). Because of the assumptions used to separate μ_a and μ'_s , the two maps are partially correlated. This leakage of the effective μ_a values into the effective μ'_s values prevents the reconstruction of quantitative maps. We note that the reconstructed values of the optical coefficients do not reproduce the actual values in the presented images. Although the lack of quantitative information is a disadvantage for some applications such as determination of blood oxygen saturation or as a screening parameter in breast mammography, most diagnostic imaging techniques used currently (magnetic resonance imaging, x-ray CT) employ only qualitative information for important diagnoses such as detecting and locating tumors.

Colak *et al.* proposed a method to recover increased resolution and quantitative results for inhomogeneities by using a set of spatially dependent deconvolutions.²⁵ Once the location and the qualitative optical properties of an inhomogeneity are determined by the use of filtered backprojection, some quantitative combination of optical properties and size of the object can be recovered through calibration by the use of maps generated by the scan of a known absorbing or scattering object between source and detector.

The Laboratory for Fluorescence Dynamics is supported by the U.S. National Institutes of Health grant RR03155 and by the University of Illinois at Urbana-Champaign. This research is also supported by the U.S. National Institutes of Health grant CA57032.

References

1. M. S. Patterson, B. Chance, and B. C. Wilson, "Time resolved reflectance and transmittance for the non-invasive measurement of tissue optical properties," *Appl. Opt.* **28**, 2331-2336 (1989).
2. S. Fantini, M. A. Franceschini, J. B. Fishkin, B. Barbieri, and E. Gratton, "Quantitative determination of the absorption spectra of chromophores in strongly scattering media: a light-emitting-diode based technique," *Appl. Opt.* **33**, 5204-5213 (1994).
3. B. C. Wilson, M. S. Patterson, and B. W. Pogue, "Instrumentation for in vivo tissue spectroscopy and imaging," in *Medical Lasers and Systems II*, D. M. Harris, C. M. Penney, and A. Katzir, eds., *Proc. SPIE* **1892**, 132-147 (1991).
4. M. S. Patterson, B. W. Pogue, and B. C. Wilson, "Computer simulation and experimental studies of optical imaging with

- photon density waves," in *Medical Optical Tomography: Functional Imaging and Monitoring*, G. J. Mueller, B. Chance, R. Alfano, S. Arridge, J. Bleuthan, E. Gratton, M. Kaschke, B. Masters, S. Svanberg, P. van der Zee, eds., Vol. IS11 of SPIE Institute Series (Society of Photo-Optical Instrumentation Engineers, Bellingham, Wash., 1993), pp. 65–86.
5. S. R. Arridge, P. van der Zee, M. Cope, and D. T. Delpy, "Reconstruction methods for infra-red absorption imaging," in *Time-Resolved Spectroscopy and Imaging of Tissues*, B. Chance and A. Katzir, eds., Proc. SPIE **1431**, 204–215 (1991).
 6. R. L. Barbour, H. L. Graber, R. Aronson, and J. Lubowsky, "Imaging of subsurface regions of random media by remote sensing," in *Time-Resolved Spectroscopy and Imaging of Tissues*, B. Chance and A. Katzir, eds., Proc. SPIE **1431**, 192–203 (1991).
 7. J. R. Singer, F. A. Grünbaum, P. Kohn, and J. Passamani Zubelli, "Image reconstruction of the interior of bodies that diffuse radiation," *Science* **248**, 990–993 (1990).
 8. K. D. Paulsen and H. Jiang, "Spatially varying optical property reconstruction using a finite element diffusion equation approximation," *Med. Phys.* **22**, 691–701 (1995).
 9. H. Jiang, K. D. Paulsen, U. L. Osterberg, B. W. Pogue, and M. S. Patterson "Optical image reconstruction using frequency-domain data: simulations and experiments," *Opt. Image Sci.* **13**, 253–266 (1996).
 10. M. A. Oleary, D. A. Boas, B. Chance, and A. G. Yodh "Experimental images of heterogeneous turbid media by frequency-domain diffusing-photon tomography," *Opt. Lett.* **20**, 426–428 (1995).
 11. B. W. Pogue, M. S. Patterson, H. Jiang, and K. D. Paulsen, "Initial assessment of a simple system for frequency domain diffuse optical tomography," *Phys. Med. Biol.* **40**, 1709–1729 (1995).
 12. M. A. Franceschini, S. Fantini, S. A. Walker, J. S. Maier, and E. Gratton, "Multi-channel optical instrument for near-infrared imaging of tissues," in *Optical Tomography, Photon Migration, and Spectroscopy of Tissue and Model Media: Theory, Human Studies, and Instrumentation*, B. Chance and R. Alfano, eds., Proc. SPIE **2389**, 264–273 (1995).
 13. J. B. Fishkin and E. Gratton, "Propagation of photon-density waves in strongly scattering media containing an absorbing semi-infinite plane bounded by a straight edge," *J. Opt. Soc. Am. A* **10**, 127–140 (1993).
 14. K. Furutsu and Y. Yamada, "Diffusion approximation for a dissipative random medium and the applications," *Phys. Rev. E* **50**, 3634–3640 (1994).
 15. J.-M. Kaltenbach and M. Kaschke, "Frequency- and time-domain modelling of light transport in random media," in *Medical Optical Tomography: Functional Imaging and Monitoring*, G. J. Mueller, B. Chance, R. Alfano, S. Arridge, J. Bleuthan, E. Gratton, M. Kaschke, B. Masters, S. Svanberg, P. van der Zee, eds., Vol. IS11 of SPIE Institute Series (Society of Photo-Optical Instrumentation Engineers, Bellingham, Wash., 1993), pp. 65–86.
 16. S. F. Feng, F. Zeng, and B. Chance, "Monte Carlo simulations of photon migration path distributions in multiple scattering media," in *Photon Migration and Imaging in Random Media and Tissues*, B. Chance and R. Alfano, eds., Proc. SPIE **1888**, 78–89 (1993).
 17. A. C. Kak and M. Slaney, *Principles of Computerized Tomographic Imaging* (IEEE, New York, 1988), pp. 49–74.
 18. R. L. Barbour, H. L. Graber, Y. Wang, J. Chang, and R. Aronson, "A perturbation approach for optical diffusion tomography using continuous-wave and time-resolved data," in *Medical Optical Tomography: Functional Imaging and Monitoring*, G. J. Mueller, B. Chance, R. Alfano, S. Arridge, J. Bleuthan, E. Gratton, M. Kaschke, B. Masters, S. Svanberg, P. van der Zee, eds., Vol. IS11 of SPIE Institute Series (Society of Photo-Optical Instrumentation Engineers, Bellingham, Wash., 1993), pp. 87–120.
 19. B. A. Feddersen, D. W. Piston, and E. Gratton, "Digital parallel acquisition in frequency domain fluorimetry," *Rev. Sci. Instrum.* **60**, 2929–2936 (1989).
 20. S. Fantini, M. A. Franceschini, and E. Gratton, "Semi-infinite-geometry boundary problem for light migration in highly scattering media: a frequency-domain study in the diffusion approximation," *J. Opt. Soc. Am. B* **11**, 2128–2138 (1994).
 21. D. A. Boas, M. A. Oleary, B. Chance, and A. G. Yodh, "Scattering of diffuse photon density waves by spherical inhomogeneities within turbid media: Analytic Solution and applications," *Proc. Natl. Acad. Sci. USA* **91**, 4887–4891 (1994).
 22. P. Krämmer, H. Bartelt, H. Fischer, and B. Schmauss, "Imaging in scattering media using the phase of modulated light sources," in *Photon Propagation in Tissues*, B. Chance, D. Delpy, and G. J. Mueller, eds., Proc. SPIE **2626**, 65–74 (1995).
 23. J. S. Maier and E. Gratton, "Frequency-domain methods in optical tomography: detection of localized absorbers and a backscattering reconstruction scheme," in *Photon Migration and Imaging in Random Media and Tissues*, B. Chance and R. Alfano, eds., Proc. SPIE **1888**, 440–451 (1993).
 24. S. Fantini, M. A. Franceschini, S. A. Walker, J. S. Maier, and E. Gratton, "Photon path distributions in turbid media: applications for imaging," in *Optical Tomography, Photon Migration, and Spectroscopy of Tissue and Model Media: Theory, Human Studies, and Instrumentation*, B. Chance and R. Alfano, eds., Proc. SPIE **2389**, 340–349 (1995).
 25. S. B. Colak, D. G. Papaioannou, G. W. 't Hooft, and M. B. van der Mark, "Optical image reconstruction with deconvolution in light diffusing media," in *Photon Propagation in Tissues*, B. Chance, D. Delpy, and G. J. Mueller, eds., Proc. SPIE **2626**, 306–315 (1995).